

New Lessons from the HI Size-Mass Relation of Galaxies

Jing Wang^{1*}, Bärbel S. Koribalski¹, Paolo Serra¹, Thijs van der Hulst²,

Sambit Roychowdhury³, Peter Kamphuis^{1,4}, Jayaram N. Chengalur⁴

¹*Australia Telescope National Facility, CSIRO Astronomy and Space Science, PO Box 76, Epping, NSW 1710, Australia*

²*University of Groningen, Kapteyn Astronomical Institute, Landleven 12, 9714 AD, Groningen, The Netherlands*

³*Max-Planck Institut für Astrophysik, D-85748 Garching, Germany*

⁴*National Centre for Radio Astrophysics, TIFR, Ganeshkhind, Pune 411007, India*

Accepted 2014 ???? ?? Received 2014 ???? ??; in original form 2014 January

ABSTRACT

We revisit the HI size-mass ($D_{\text{HI}}\text{-}M_{\text{HI}}$) relation of galaxies with a sample of more than 500 nearby galaxies covering over five orders of magnitude in HI mass and more than ten B -band magnitudes. The relation is remarkably tight with a scatter $\sigma \sim 0.06$ dex, or 14%. The scatter does not change as a function of galaxy luminosity, HI richness or morphological type. The relation is linked to the fact that dwarf and spiral galaxies have a homogenous radial profile of HI surface density in the outer regions when the radius is normalised by D_{HI} . The early-type disk galaxies typically have shallower HI radial profiles, indicating a different gas accretion history. We argue that the process of atomic-to-molecular gas conversion or star formation cannot explain the tightness of the $D_{\text{HI}}\text{-}M_{\text{HI}}$ relation. This simple relation puts strong constraints on simulation models for galaxy formation.

Key words: intergalactic medium; galaxies

1 INTRODUCTION

Galaxies are complex ecosystems of gas, stars and dark matter governed by the interplay of different processes. Yet, they may be simpler than expected as many galaxy properties are well correlated with one another (e.g. Kauffmann et al. 2003, Tremonti et al. 2004, Catinella et al. 2010), with mass and environment being probably the most controlling parameters (Peng et al. 2010). Scaling relations are especially prevalent in HI-rich, star-forming galaxies as they usually have a relatively smooth history for assembling their mass (Disney et al. 2008). While the Tully-Fisher relation may be one of the best-known HI-based scaling relations, galaxies also show tight correlations between their HI size and mass.

The relation between HI mass (M_{HI}) and the diameter of the HI disk (D_{HI}) defined at a surface density (Σ_{HI}) of $1 M_{\odot} \text{pc}^{-2}$ was investigated by Broeils & Rhee (1997, B97 hereafter) and parametrised as:

$$\log D_{\text{HI}} = 0.51 \log M_{\text{HI}} - 3.32 \quad (1)$$

where D_{HI} is in unit of kpc and M_{HI} is in unit of $M_{\odot} \text{pc}^{-2}$. Later studies confirmed the $D_{\text{HI}}\text{-}M_{\text{HI}}$ relation (also referred to as the HI size-mass relation in this paper) with other

samples: Verheijen & Sancisi. (2001) for spiral galaxies from the Ursa Major cluster, Swaters et al. (2002) for dwarf and spiral galaxies, Begum et al. (2008) for dwarf galaxies, Noordermeer et al. (2005) for early-type disk galaxies and Wang et al. (2013) for massive spiral galaxies. B97 pointed out that, because the slope is close to 0.5 the relation indicates that the average HI surface density Σ_{HI} is nearly constant among different types of galaxies. This simple interpretation might be the reason why this relation has not been investigated further, despite the availability of resolved HI images covering a much larger range in M_{HI} , D_{HI} and other galaxy properties than the individual studies mentioned above.

This idea is further supported by the finding that galaxies have a sharp saturation of Σ_{HI} at $\sim 9 M_{\odot} \text{pc}^{-2}$, where gas at higher surface densities has been converted to molecular gas (Bigiel et al. 2008). However, there is one order of magnitude change in Σ_{HI} between the saturation value and where D_{HI} is measured, while the $D_{\text{HI}}\text{-}M_{\text{HI}}$ relation typically has a scatter of less than 0.1 dex. Different galaxies need to have an almost uniform distribution function of Σ_{HI} in order to form a very tight $D_{\text{HI}}\text{-}M_{\text{HI}}$ relation. This is not directly expected because Σ_{HI} is regulated by conversion to molecular gas which should vary significantly between galaxies (Leroy et al. 2008). Moreover, it is worth pointing out that the $D_{\text{HI}}\text{-}M_{\text{HI}}$ relation is not directly linked with the averaged

* Email: j.wang@csiro.au

Σ_{HI} because a significant fraction of M_{HI} is found outside D_{HI} (this is especially true for early-type galaxies; Serra et al. 2012).

In this paper, we will study the scatter and slope of the $D_{\text{HI}}-M_{\text{HI}}$ relation using a sample of galaxies with as wide as possible a range in HI size, mass and other properties. We will explore possible explanations for the tightness of the HI mass-size relation by investigating its dependence on other parameters. We assume a Λ CDM cosmology with $\Omega_m = 0.3$, $\Omega_{\text{lamba}bda} = 0.7$ and $h = 0.7$ throughout the paper.

2 SAMPLE & DATA

We compiled HI interferometric data from 15 projects and summarise the sample names, relevant galaxy numbers, types and environment in Table 1. As we will explain below, only galaxies with reliable D_{HI} measurements are considered.

We take the values of D_{HI} from published catalogues for five of the samples. A few galaxies in Ursa Major do not have D_{HI} measurements and are excluded. Because the Kovač et al. (2009, K09 hereafter, see Table 1) sample has very faint systems, we exclude those galaxies with flux uncertainties larger than 15%.

We directly measure D_{HI} using the procedure of Wang et al. (2014) for the other ten samples for which we have access to the HI intensity maps. Whenever possible, we use HI images produced with natural weighting in order to have high sensitivity to the extended gas. D_{HI} is measured as the major axis of a fitted ellipse to the HI distribution where the azimuthally averaged Σ_{HI} reaches $1 M_{\odot} \text{pc}^{-2}$. For each galaxy from the dwarf and spiral samples, the elliptical shape (position angle and ellipticity) is determined from the HI maps, based on the second order moments of the pixel distributions where $\Sigma_{\text{HI}} > 1 M_{\odot} \text{pc}^{-2}$. For the early-type galaxies from Atlas3D we use the elliptical shapes obtained by Serra et al. (2014) from tilted ring fits to the velocity fields. These are more reliable in the case of a disturbed disk morphology, as frequently observed in early type galaxies (Serra et al. 2012, 2014). A similar argument applies to VIVA galaxies in the Virgo Cluster, and the kinematic elliptical shapes are taken from Chung et al. (2009). We note that using elliptical shapes determined from HI images (as we do for the dwarf and spiral galaxies) for the Atlas3D and VIVA galaxies adds some scatter to but does not significantly change the results presented in this paper. In the final step, D_{HI} are corrected for beam smearing effects based on a Gaussian approximation: $D_{\text{HI}} = \sqrt{D_{\text{HI},0}^2 - B_{\text{maj}} \times B_{\text{min}}}$, where D_{HI} and $D_{\text{HI},0}$ are the corrected and uncorrected HI sizes, and B_{maj} and B_{min} are the major and minor axes of the HI beam.

For all samples we further select galaxies with $D_{\text{HI}} > 2 B_{\text{maj}}$. The samples with low resolution data (LVHIS, WHISP, Bluedisk, Atlas3D, VGS) or very small galaxies (FIGGS, K09) are affected by this selection criterion and contain fewer galaxies in this paper than published in the reference papers (Table 1).

For galaxies with large angular sizes, extended HI flux might be missing in the interferometric data due to (a) a lack of short baselines, (b) small field of view. Based on the information given in the reference papers, we try our best

to exclude these galaxies. For LVHIS, THINGS, LITTLE THINGS, FIGGS and VIVA, comparisons between interferometric and single dish HI mass measurements have been presented in the relevant reference papers and we only select those galaxies where the two HI mass measurements agree within 15%. For the WHISP samples we select galaxies with D_{HI} smaller than $400''$, as Swaters et al. (2002) estimated that the missing flux in these galaxies is less than 10% compared to single-dish fluxes. Galaxies from other samples do not appear to have a missing flux problem.

After these selection criteria, there are in total 542 galaxies left (501 unique ones) and they serve as our analysis sample (the sample for Fig. 1, Section 3). We note that the overlapping galaxies have consistent D_{HI} measurements in units of arcsec (the rms scatter of the differences is less than 0.07 dex). We have access to HI images for 330 of the 542 images (this sub-sample is used in Fig. 4, Section 3). For 293 of the 542 galaxies $D_{\text{HI}} > 3 B_{\text{maj}}$, such that the radial profile of Σ_{HI} is reasonably resolved (this sub-sample is used in Fig. 2, Section 3).

We retrieve the B -band magnitudes (M_B) and B -band diameter D_{25} (the major axis for the $25 \text{ mag arcsec}^{-2}$ isophote) from the SIMBAD astronomical database² for 455 of the 501 unique galaxies in our sample. We estimate M_B for the Bluedisk galaxies from the g -band magnitudes with a correction based on the $g-r$ colour (Jester et al. 2005). We also use g band D_{25} to approximate the B -band D_{25} for the Bluedisk galaxies. The g - and r -band data are taken from SDSS (Sloan Digital Sky Survey, York et al. 2000). Ultimately, we are able to obtain optical parameters for 494 of the galaxies (the sub-sample for Fig. 3, Section 3). These optical measurements are inhomogeneous, and the uncertainties are substantial (see, e.g., West et al. (2010) for a discussion of the difficulties associated with measuring optical magnitudes for extended galaxies such as these). However, a full reprocessing of the optical data is beyond the scope of the current work. Therefore, the results based on M_B and D_{25} should be treated with caution.

We list the first five galaxies of our full sample along with their HI and optical parameters investigated in this paper in Table 2. A full version of the catalogue is available online.

In addition to the main sample, we also collect HI diameters and masses for the Milky Way (MW), the Small Magellanic Cloud (SMC), the Large Magellanic Cloud (LMC), M31 and a few other special galaxies (Table 3). SMC and LMC are interacting with the MW, Malin 1, Malin 2, NGC 765 and HIZOA J0836-43 are known for their extremely high M_{HI} , and Leo T has a very low M_{HI} . We include these objects to test whether the $D_{\text{HI}}-M_{\text{HI}}$ relation extends to these extreme HI masses.

3 RESULTS

3.1 The $D_{\text{HI}}-M_{\text{HI}}$ relation

We present the $D_{\text{HI}}-M_{\text{HI}}$ relation in Fig. 1. The different samples include dwarf galaxies, spiral galaxies, early-type disk galaxies (Atlas3D and WHISP Sa) and they cover a

² <http://simbad.u-strasbg.fr/simbad/>

Table 2. Galaxies in the analysis sample (Section 2)*

galaxy	D _{HI} kpc	log M _{HI} M _⊙	distance Mpc	PA ^a deg	b/a ^b	M _B mag	D ₂₅ kpc	sample	ref ^c for D _{HI}
UGC731	15.20	8.87	8.0	-9.2	0.56	-13.08	5.09	WHISP(S)	this work
UGC1281	9.76	8.51	5.5	-52.6	0.30	-15.89	7.15	WHISP(S)	this work
UGC2023	12.98	8.65	10.1	-29.5	0.90	-15.50	4.99	WHISP(S)	this work
UGC2034	18.57	8.93	10.1	-43.3	0.90	-15.25	7.34	WHISP(S)	this work
UGC2053	12.94	8.75	11.8	-41.2	0.86	-15.16	7.01	WHISP(S)	this work

*It does not include galaxies from the B97 sample, for which we refer the readers to B97 for a similar table. Here we list the first 5 rows of the table, and the full version is available online.

^aHI disk position angle, measured from north through east.

^bHI disk axis ratio.

^cReference paper for D_{HI} and M_{HI}.

Table 1. HI interferometric data from 15 projects.

Sample	N ^a	Type ^b	env ^c	reference
B97*	107	S, dIrr	-	Broeils & Rhee (1997)
WHISP (S)	59	S, dIrr	-	Swaters et al. (2002)
LWHIS ^d	56	S, dIrr	-	Koribalski (2008)
THINGS	19	S, dIrr	-	Walter et al. (2008)
Bluedisk	39	S	<i>iso</i>	Wang et al. (2013)
Diskmass*	28	S	-	Martinsson et al. (2016)
VGS	14	S	<i>v</i>	Kreckel et al. (2012)
Ursa Major*	38	S	<i>c</i>	Verheijen & Sancisi (2001)
VIVA	36	S	<i>c</i>	Chung et al. (2009)
LITTLE THINGS	39	dIrr	<i>iso</i>	Hunter et al. (2012)
K09*	23	dIrr	-	Kovač et al. (2009)
L14*	16	dIrr	-	Lelli et al. (2014)
FIGGS	25	dIrr	-	Begum et al. (2008)
WHISP (Sa)	41	Sa	-	Noordermeer et al. (2002)
Atlas3D	9	E/S0	-	Serra et al. (2012, 2014)

^aNumber of galaxies included in the full analysis sample.

^bS for spiral galaxies.

^cEnvironment: *iso* for being relatively isolated, *c* for galaxy cluster, *v* for voids in the cosmological large scale structure.

^dThe Local Volume HI Survey (LVHIS, Koribalski 2008) includes HI data from Westmeier et al. (2011, 2013) and Ryder et al. (1995).

*D_{HI} are directly taken from the reference paper.

Table 3. HI properties for a few individual galaxies.

name	log M _{HI} M _⊙	D _{HI} kpc	Distance Mpc	reference
Malin 1	10.66	220 ^a	329	Matthews et al. (2001)
Malin 2	10.52	69 ^a	183	Matthews et al. (2001)
J0836-43 ^c	10.88	120	148	Donley et al. (2006)
NGC765	10.67	240 ^b	72	Portas et al. (2010)
MW	9.9	42	-	Kalberla & Kerp (2009)
M31	9.63	42	0.79	Chemin et al. (2009)
LMC	8.68	18.6	0.05	Staveley-Smith et al. (2003)
SMC	8.62	10.4	0.06	Staveley-Smith et al. (1998)
Leo T	5.44	0.3	0.42	Ryan-Weber et al. (2008)

^a for half light diameter.

^bHI diameter is measured at $N_{\text{HI}} = 2 \times 10^{19}$ atoms cm⁻².

^cThe full name is HIZOA J0836-43.

range of environments, but they all lie perfectly on the same D_{HI}-M_{HI} relation. We perform a robust linear fitting to the data points and obtain the relation:

$$\log D_{\text{HI}} = (0.506 \pm 0.003) \log M_{\text{HI}} - (3.293 \pm 0.009), \quad (2)$$

which is very close to the one found by B97. The rms scatter around the relation is only ~ 0.06 dex (14%). The intercept of $3.3 \sim 0.5(\log M_{\text{HI}} - 2 \log D_{\text{HI}}) = 0.5 \log M_{\text{HI}}/D_{\text{HI}}^2$ indicates a uniform characteristic HI surface density

$$\Sigma_{\text{HI},c} = 4 \frac{M_{\text{HI}}}{\pi D_{\text{HI}}^2} = 5.07 M_{\odot} \text{ pc}^{-2} \quad (3)$$

for different galaxies. We emphasise that $\Sigma_{\text{HI},c}$ is not the actual average Σ_{HI} , because D_{HI} does not enclose the entire HI disk and M_{HI}. We will come back to this point later.

HIZOA J0836-43 and Leo T lie at the two extreme ends of the relation, thus the D_{HI}-M_{HI} relation extends from M_{HI} of a few times $10^5 M_{\odot}$ to nearly $10^{11} M_{\odot}$. We only have HI effective diameters for Malin 1 and 2, and the diameter at a column density of $2 \times 10^{19} \text{ cm}^{-2}$ for NGC 765, but these size measurements lie reasonably close to the D_{HI}-M_{HI} relation. It is expected that the MW and M31 lie on the D_{HI}-M_{HI} relation, as they are normal spiral galaxies. The LMC and SMC are known to be tidally interacting with the MW, but they lie within 3σ from the D_{HI}-M_{HI} relation. We note that equation 2 is also very close to the relations published in other studies (Verheijen & Sancisi 2001, Swaters et al. 2002, Noordermeer et al. 2002, Begum et al. 2008). The very small differences in coefficients (less than 15%) are likely to be caused by different ways of measuring D_{HI}.

The D_{HI}-M_{HI} relation suggests that different galaxies have similar distributions of HI surface densities. To understand this better, we present the median HI radial profiles (with radius normalised by $R_{\text{HI}} = 0.5D_{\text{HI}}$) for different samples (Fig. 2). We find that the median profiles of different dwarf and spiral galaxy samples have a homogeneous shape in the outer regions around the position of R_{HI} (also see Wang et al. 2014). The shape is well described by an exponential function with a scale length $\sim 0.2 R_{\text{HI}}$. The only exceptions are the early-type disk galaxies from the Atlas3D and WHISP samples, which have a larger HI scalelength in units of R_{HI} compared to other galaxies. However, they also have lower Σ_{HI} in the inner region, which conspires to put the objects on the same D_{HI}-M_{HI} relation as other galaxies. We run a K-S test on the distributions of scatter from the

$D_{\text{HI}}\text{-}M_{\text{HI}}$ relation for the early-type disk and other galaxies. The possibility that the two distributions are different is just 36%. We will discuss the Σ_{HI} distribution of these early-type disk galaxies further in Section 4.

These homogeneous HI profiles also support $\Sigma_{\text{HI},c}$ (Equation 3) as an indicator of the averaged Σ_{HI} for dwarf and spiral galaxies in general. However, this indicator is not applicable to the early-type disk galaxies because of their different Σ_{HI} distributions.

In Fig. 3, we investigate the vertical distance of galaxies from the mean $D_{\text{HI}}\text{-}M_{\text{HI}}$ relation as a function of M_{HI} , M_B , HI mass to optical light ratio M_{HI}/L_B and HI to optical size ratio D_{HI}/D_{25} . Galaxies in the sample cover a wide range of these properties, but their median distance and scatter around the $D_{\text{HI}}\text{-}M_{\text{HI}}$ relation do not vary with them. As can be seen from Fig. 1, the low M_{HI} end is dominated by galaxies from LITTLE THINGS and FIGGS samples, which targeted very low mass dwarf galaxies (Begum et al. 2008, Hunter et al. 2012). The B -band magnitude (luminosity) can also be viewed as a rough indicator of stellar mass (although the exact stellar mass-to-light ratio depends on the stellar populations of galaxies, Bell et al. 2003). So the first two panels compare the scatter and offset of galaxies with different masses from the $D_{\text{HI}}\text{-}M_{\text{HI}}$ relation. In the third and fourth panels, M_{HI}/L_B and D_{HI}/D_{25} are measures of HI-richness in these galaxies.

Because measuring D_{HI} at $1 M_{\odot} \text{pc}^{-2}$ is a subjective choice, we explore the properties of $D_{\text{HI}}\text{-}M_{\text{HI}}$ relations with sizes defined at different surface densities (Fig. 4). We find the scatter of the relations minimized when the HI size is measured at surface densities between 1 and $2 M_{\odot} \text{pc}^{-2}$ (top panel). At lower or higher surface densities the scatter gradually increases. When D_{HI} is measured at Σ_{HI} of $2 M_{\odot} \text{pc}^{-2}$, the enclosed HI mass is only 70% of the total (panel 3), but the scatter and slope of the size-mass relation do not change much compared to the relation calibrated at $1 M_{\odot} \text{pc}^{-2}$ (panel 1 and 2). This is consistent with the finding of homogeneous HI profile shapes in the outer regions of galaxies, and suggests that the $D_{\text{HI}}\text{-}M_{\text{HI}}$ relation works not because D_{HI} encloses most of the HI mass in a galaxy but because galaxies have similar distributions of Σ_{HI} . An advantage of measuring D_{HI} at $1 M_{\odot} \text{pc}^{-2}$ is that it is more easily measurable for small HI disks that are close to being unresolved (panel 4). To summarise, D_{HI} defined at $1 M_{\odot} \text{pc}^{-2}$ presents a good balance between having a good correlation with the HI mass, enclosing most of the HI in a galaxy and being measurable for most of the galaxies.

We point out that the observed scatter in the $D_{\text{HI}}\text{-}M_{\text{HI}}$ relation is a combination of the intrinsic scatter and errors in the size measurements, and should be viewed as an upper limit on the intrinsic scatter. Uncertainties in galaxy distance estimates do not affect the $D_{\text{HI}}\text{-}M_{\text{HI}}$ relation very much. This is because the slope of the relation is close to 0.5, and as a result uncertainties in distance only move galaxies along the $D_{\text{HI}}\text{-}M_{\text{HI}}$ relation. We have tested this by randomly changing the distances by up to 50%, and the slope, intercept and scatter of the $D_{\text{HI}}\text{-}M_{\text{HI}}$ relation change by less than 1.5%.

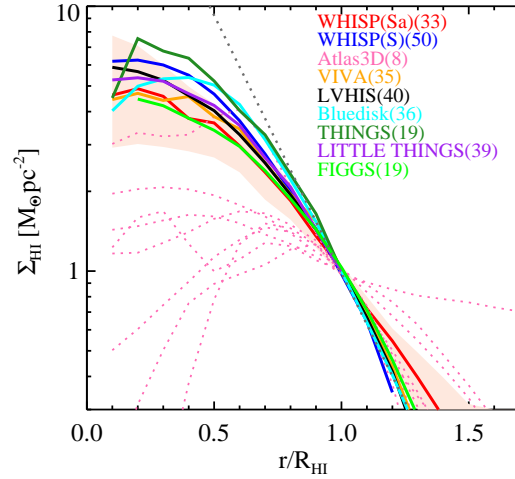


Figure 2. Σ_{HI} radial profiles for nine samples; only galaxies 3 times larger than the respective interferometric beam are included here. We display the median profile for each sample, except for Atlas3D where we show the individual profiles. We also show the 25 and 75 percentile of profiles for the WHISP (Sa) sample (the red shaded region). The dotted black line is an exponential fit to the homogeneous outer profiles of the samples excluding the Atlas3D and WHISP (Sa) samples. The VGS sample is not present because only 5 galaxies are large enough for measuring the profile.

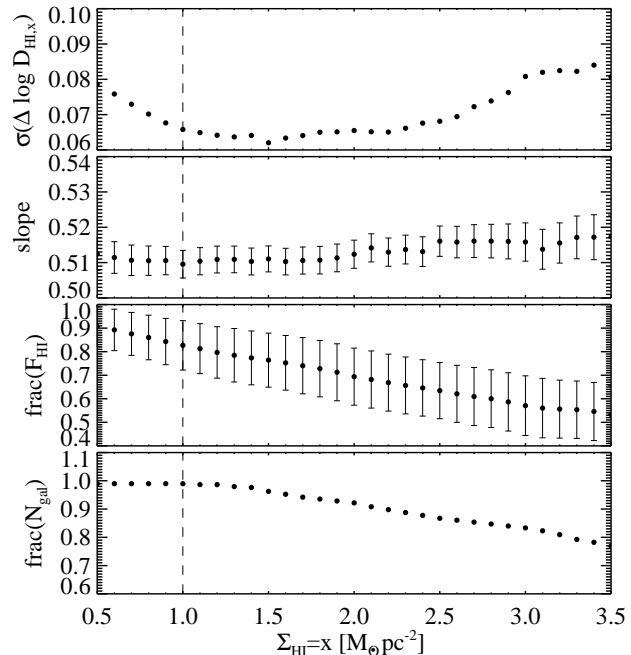


Figure 4. Comparison of different $D_{\text{HI}}\text{-}M_{\text{HI}}$ relations with D_{HI} defined at a range of HI surface brightness densities. The measurements are based on the 10 samples where we have HI maps. From top to bottom: the scatters and slopes of the relations, the fraction of total fluxes enclosed in D_{HI} and the fraction of galaxies with measurable D_{HI} are shown.

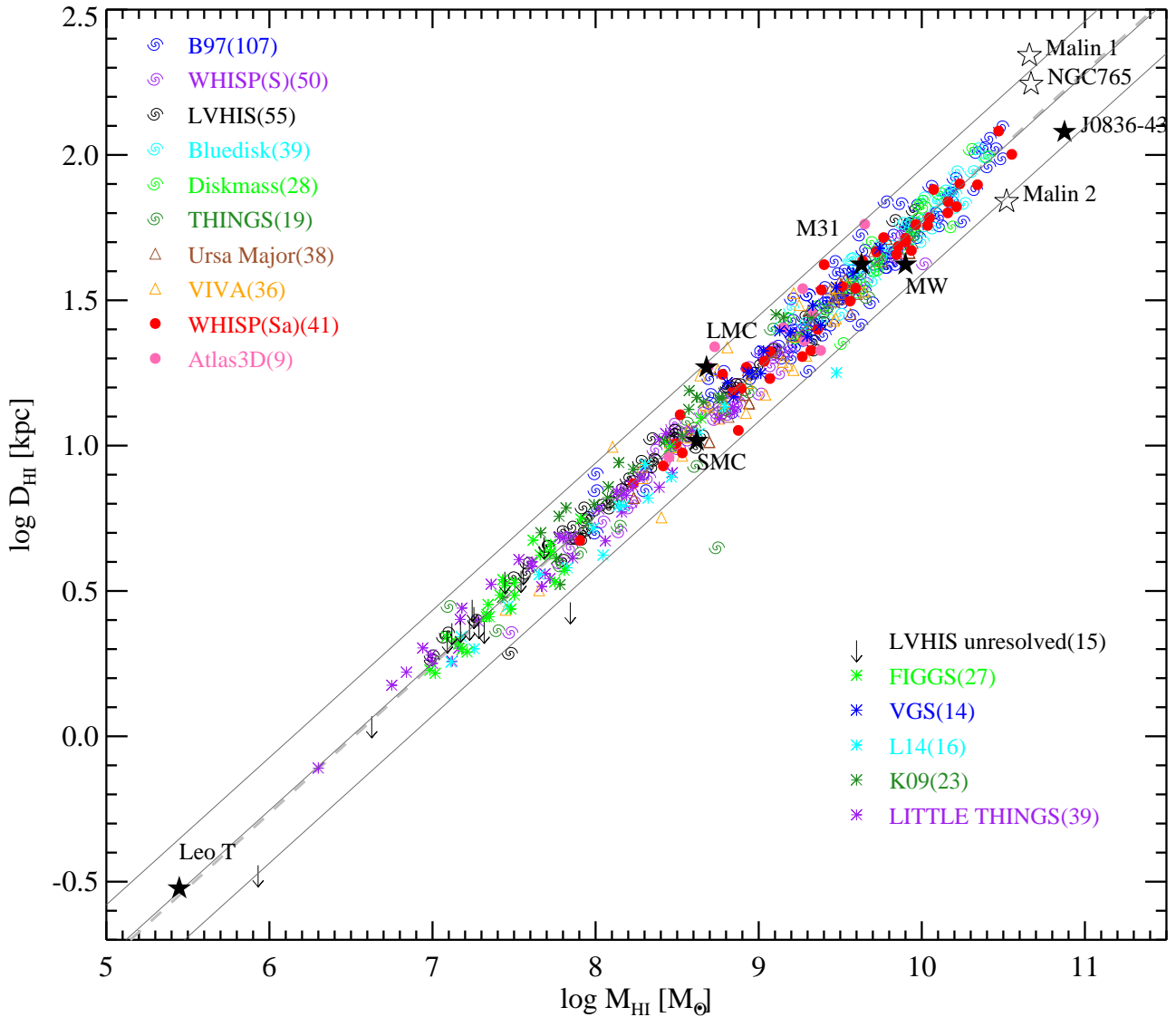


Figure 1. The $D_{\text{HI}}-M_{\text{HI}}$ relation for 562 galaxies from 15 interferometric data sets (see Table 1). We also show D_{HI} upper limits for 15 unresolved galaxies from LVHIS. Furthermore, nine special individual galaxies have been shown in stars (see Table 2). The solid lines represent the best-fit linear relation and the $3\text{-}\sigma$ scatter. The dashed line represents the B97 relation.

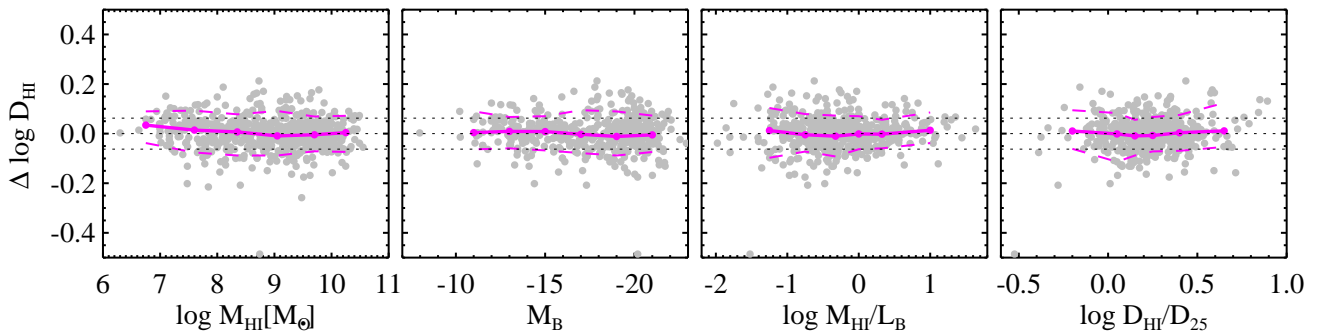


Figure 3. Vertical offset of galaxies from the $D_{\text{HI}}-M_{\text{HI}}$ relation as a function of M_{HI} , M_{B} , $M_{\text{HI}}/L_{\text{B}}$, and D_{HI}/D_{25} . The solid magenta lines show the median, and the dashed magenta lines show the 10 and 90 percentiles of the distribution. The dotted black lines mark the position of 0 and 1σ scatter measured in Figure 1. The optical properties are taken from the Simbad astronomical database and are inhomogeneous.

3.2 Outliers

There are seven extreme outliers deviating by more than 3σ from the $D_{\text{HI}}\text{-}M_{\text{HI}}$ relation in Fig. 1 (one of them is an upper limit on D_{HI} for the unresolved galaxy ESO 149-G003). We display the HI intensity images of the objects for which we have access to the data (see Fig. 5). NGC 4380 and NGC 4694 are in the Virgo cluster. NGC 4380 is a highly HI-deficient galaxy with a deficiency factor higher than 99.7% (3σ) of galaxies with the same Hubble type and size (Cortese et al. 2010). NGC 4694 is in the middle of a merger event (Chung et al. 2009). NGC 5237 shows obvious signs of being disturbed (Koribalski et al. 2016). NGC 3941 has an HI disk that is counter-rotating with the stellar disk (Serra et al. 2014). It also shows an asymmetric distribution of high density HI regions on the disk. NGC 4826 (Braun et al. 1994) and NGC 4449 (Hunter et al. 1998, HI image not shown) host counter-rotating double HI disks. We can see that NGC 4826 has a strikingly large HI low surface density disk surrounding a compact core. The remaining outlier is ESO 149-G003, which is barely resolved, also shows hints of hosting counter-rotating double HI disks from three-dimensional kinematic analysis (Kamphuis et al. in prep). To summarise, none of the extreme outliers for the $D_{\text{HI}}\text{-}M_{\text{HI}}$ relation are normal HI-rich galaxies, and many of them show kinematical abnormalities.

On the other hand, we find that not all the morphologically or kinematically abnormal galaxies in our sample deviate significantly from the $D_{\text{HI}}\text{-}M_{\text{HI}}$ relation. For example, NGC 6798 is also known to have an HI disk that counter-rotates with respect to the stellar disks (Serra et al. 2014), but we find it to lie within the 3σ scatter from the $D_{\text{HI}}\text{-}M_{\text{HI}}$ relation. We show HI images of two examples of morphologically disturbed galaxies whose offsets from the $D_{\text{HI}}\text{-}M_{\text{HI}}$ relation are less than 3σ . In the left panel of Fig. 6, NGC 4294 and NGC 4299 are interacting with each other but they both lie within 2σ from the $D_{\text{HI}}\text{-}M_{\text{HI}}$ relation (similar for the SMC and the LMC which are interacting with the MW, as shown in Fig. 1). In the right panel, as demonstrated and discussed in Chung et al. (2009), NGC 4402 is possibly affected by ram pressure stripping such that one end of the HI disk is truncated within the optical disk and the other end has a tail. But its offset from the mean $D_{\text{HI}}\text{-}M_{\text{HI}}$ relation is only 0.01 dex. In both panels (three galaxies), the $1 M_{\odot} \text{ pc}^{-2}$ contours are not significantly disturbed by the environmental effects. This suggests that HI gas with $\Sigma_{\text{HI}} > 1 M_{\odot} \text{ pc}^{-2}$ might be highly stable against tidal or ram pressure effects, or the timescale for disturbed galaxies to be settled again might be very short. A larger and more complete sample of disturbed galaxies is needed to draw a firm conclusion.

4 DISCUSSION

We have presented a remarkably tight $D_{\text{HI}}\text{-}M_{\text{HI}}$ relation with the largest sample examined to date. The sample covers around five orders of magnitude in HI mass, ten B -band magnitudes, three orders of magnitude in M_{HI}/L_B , and one order in D_{HI}/D_{25} . We have investigated whether the scatter about the $D_{\text{HI}}\text{-}M_{\text{HI}}$ relation depends on any of these parameters but found that it does not. We have found that the $D_{\text{HI}}\text{-}M_{\text{HI}}$ relation is a consequence of the self-similar Σ_{HI}

radial profiles of galaxies. In this section we discuss the implications of these results on the mechanisms that drive the $D_{\text{HI}}\text{-}M_{\text{HI}}$ relation.

4.1 Σ_{HI} in dwarf, spiral and early-type disk galaxies

We find that dwarf and spiral galaxies have a homogeneous Σ_{HI} radial profile shape when the radius is normalised by D_{HI} . This is a strong constraint on the distribution of Σ_{HI} in galaxies, which implies that dwarf and spiral galaxies share a common mechanism in regulating the radial distribution of HI.

Early-type disk galaxies show larger scale-length in units of D_{HI} (Fig. 2) which indicates a different gas assembly history compared to dwarf and spiral galaxies. A more extended HI distribution is often connected with recent accretion events. In galaxy formation models under a Λ CDM cosmology, gas that is accreted at a later time has higher specific angular momentum and settles in the outer region of galaxy disks, resulting in larger characteristic sizes (Mo et al. 1998). Under the scheme of such models, if an early-type disk galaxy only contains recently accreted gas, the scalelength will be naturally larger than the average of HI-rich spiral galaxies which contain both earlier and recently accreted HI gas. The external origin of the HI in a large fraction of E/S0s is confirmed by the frequent kinematical misalignment between HI and stars (Serra et al. 2014). This conclusion does not necessarily hold for early-type galaxies where the HI is detected on a compact disk. These disks are usually co-rotating with the stars and their Σ_{HI} profile can not be accurately measured with current data.

The investigation on Σ_{HI} provides constraints, but not a physical explanation for the $D_{\text{HI}}\text{-}M_{\text{HI}}$ relation. Below we will discuss the possible astrophysical drivers. Because it is possible that the early-type disk galaxies in our sample have a special assembly history, we decide to exclude them in the following discussion for general HI-rich galaxies, although they lie coincidentally on the same $D_{\text{HI}}\text{-}M_{\text{HI}}$ relation as other galaxies.

4.2 What is the driver for the $D_{\text{HI}}\text{-}M_{\text{HI}}$ relation?

It is surprising that low-mass dwarf and high-mass spiral galaxies lie on the same $D_{\text{HI}}\text{-}M_{\text{HI}}$ relation and exhibit similar scatter from the relation.

As we discussed in Section 3, the intercept of the $D_{\text{HI}}\text{-}M_{\text{HI}}$ relation indicates a characteristic $\Sigma_{\text{HI},c}$ (Equation 3) and can be viewed as an approximate measure of the average Σ_{HI} for dwarf and spiral galaxies. In galaxy formation models, Σ_{HI} is regulated by the HI-to- H_2 conversion process (Fu et al. 2012, Lagos et al. 2011). In most models, the HI-to- H_2 conversion efficiency $M_{\text{H}_2}/M_{\text{HI}}$ depends on the mid-plane pressure (e.g. Blitz & Rosolowsky 2006, Ostriker et al. 2010) and metallicity (e.g. Sternberg et al. 2014). Both mid-plane pressure and metallicity are correlated with the stellar mass (luminosity) of galaxies (Kauffmann et al. 2003, Kirby et al. 2013). As a result, $M_{\text{H}_2}/M_{\text{HI}}$ is on average much lower in dwarf galaxies than in massive spiral galaxies (supported by observations, e.g. Leroy et al. 2008), and we would thus expect a shift in the intercepts of the $D_{\text{HI}}\text{-}M_{\text{HI}}$ relation ($\Sigma_{\text{HI},c}$)

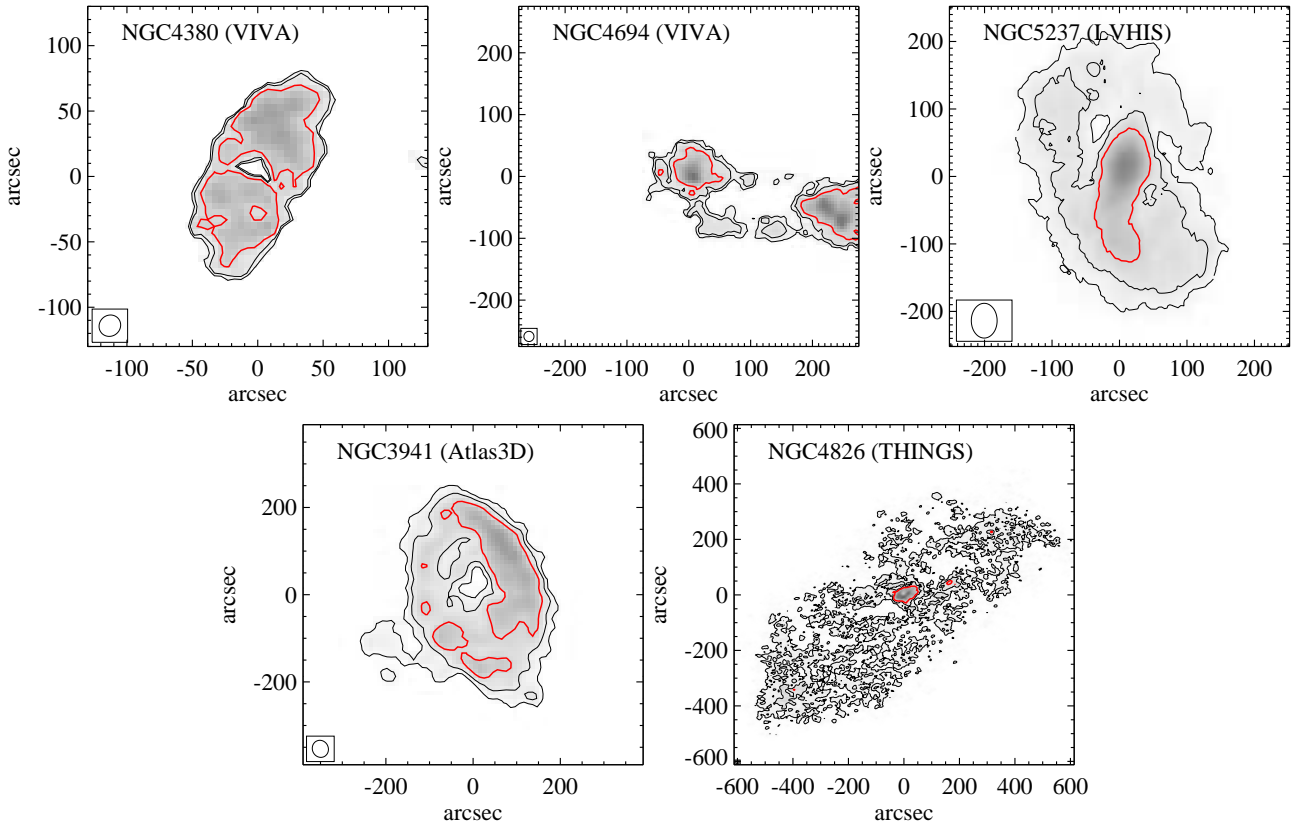


Figure 5. HI intensity images for extreme outliers in Fig. 1 (see Section 3). The contour levels are 0.3, 0.5, 1, 5 and $10 M_{\odot} \text{pc}^{-2}$, and the $1 M_{\odot} \text{pc}^{-2}$ contour is highlighted with red colour. The galaxy name and the related HI survey are in the left-top corner of each panel. The beam size is shown at the left-bottom corner of each panel.

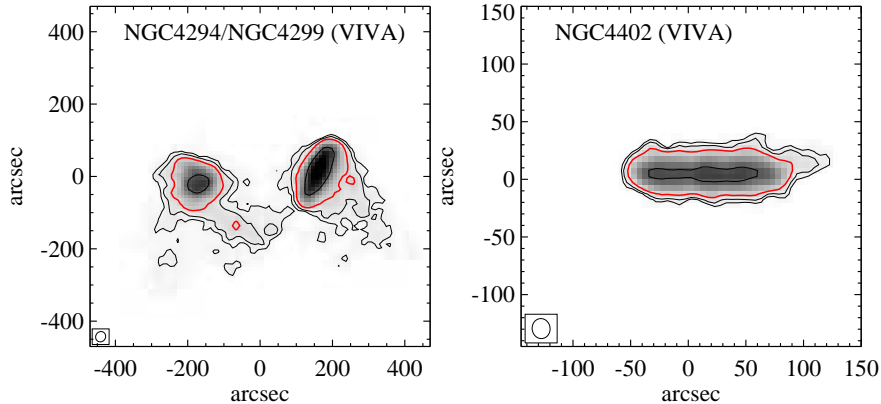


Figure 6. Example of disturbed galaxies which lie within 3σ scatter from the mean $D_{\text{HI}}-M_{\text{HI}}$ relation. Otherwise similar to Fig. 5.

for galaxies with different stellar masses (luminosities). This is not observed in our analysis.

Because H_2 and star formation are closely correlated (Krumholz et al. 2011), the H I -to- H_2 conversion should be reflected in the star formation activity. Consistent with the mass dependence of $M_{\text{H}_2}/M_{\text{HI}}$, the HI related star forming efficiency SFR/M_{HI} is lower for galaxies with lower stellar masses (Huang et al. 2012). Moreover, the star formation histories of dwarf galaxies (in the past 1 Gyr) are observed to be much more bursty (discontinuous) than those in massive star-forming galaxies (Kauffmann et al. 2014). In the extremely low mass galaxies, star formation can happen in a highly stochastic way (Matteucci et al. 1983). Starburst

galaxies have significantly enhanced star formation efficiency compared to normal star forming galaxies (Jaskot et al. 2015). Moreover, one of the scenarios to explain the bursty star formation history of dwarf galaxies is non-continuous gas accretion (Kauffmann et al. 2006) which may temporarily cause an excess of HI gas with respect to the star formation rate. For these reasons, we would expect a larger scatter on the $D_{\text{HI}}-M_{\text{HI}}$ relation for the dwarf galaxies when compared to massive spiral galaxies if the HI conversion process is the major regulator for Σ_{HI} in galaxies. This is also not observed in our analysis.

There is evidence that the local star formation efficiency in HI dominated regions is similar for different types

of galaxies (Bigiel et al. 2010, Roychowdhury et al. 2015, Yim & van der Hulst in prep), so the possible influence of star formation in the HI dominated regions should be similar for different galaxies. However it is unclear how this would affect Σ_{HI} , for the star formation depletion time at these low gas surface densities are several times the Hubble time.

All these suggest that the HI-to-H₂ conversion process or star formation is not likely to be the major or only driver for the D_{HI}-M_{HI} relation.

We have further shown that the D_{HI}-M_{HI} relation and scatter do not change between the highly HI-dominated galaxies ($M_{\text{HI}}/L_B \geq 10$ or $D_{\text{HI}}/D_{25} \geq 4$) and the relatively HI-poor galaxies. This implies that the size and mass of the HI disk grow or shrink simultaneously in a well regulated way when the HI gas is accreted, consumed or removed.

To summarise, we are not able to identify the main driver for the universal D_{HI}-M_{HI} relation, however, we obtain several constraints on the puzzle with the data presented in this paper. We find that the D_{HI}-M_{HI} relation does not depend on the luminosity or HI richness of the galaxies. Especially, the HI-to-H₂ conversion process or star formation is not likely to be the key driver for the relation.

4.3 Future prospects

Considering the limited numbers of galaxy properties explored here, in the future, other galaxy properties may reveal a correlation with the scatter about the D_{HI}-M_{HI} relation. Quantifying the kinematics of gas at each radius might provide us with more insight, as the baryonic mass profile shape, the angular momentum and gas inflow should play a role in shaping the HI distribution (e.g. Meurer et al. 2013).

We will also gain insight into the question by combining observations with numerical simulations. Different ways of implementing supernova (SN) feedback in models can produce different distributions of Σ_{HI} (Davé et al. 2013, Bahé et al. 2016). For example, it was found that as a consequence of the feedback implementation, many galaxies from the EAGLE simulation have unrealistic large holes in their HI disks and the HI radial profiles are too shallow compared to real galaxies (Bahé et al. 2015). Especially, SN feedback may also be mass dependent. It works through energy output in low-mass galaxies, and through angular momentum flux in high-mass systems (Hopkins et al. 2012). The reason why we do not observe a luminosity dependent shift in the intercept of the D_{HI}-M_{HI} relation could be that different mass dependent processes cancel out each other. The magnetic field and the cosmic ray pressure may also play a role in pushing gas around (Parker 1969, Lou et al. 2003). Studying the M_{HI}-D_{HI} relation will put strong constraints on implementing and balancing the different processes in galaxy formation models.

We point out that we are working on a mostly HI-selected and inhomogeneous sample of galaxies. Although we find that on average galaxies with very low M_{HI}/L_B or small D_{HI}/D_{25} show no differences in slope and scatter on the D_{HI}-M_{HI} relation, a more complete census of galaxies based on a homogeneously defined sample of galaxies will be useful to confirm or test our result. In particular, Brown et al. (2015) found a bimodality of the HI mass distribution at fixed stellar mass through stacking HI spectra from the ALFALFA sample (The Arecibo Legacy Fast ALFA Survey,

Giovanelli et al. 2005). Most of the galaxies in our sample should belong to the HI-rich sequence. It will be interesting to measure the D_{HI}-M_{HI} relation for galaxies on the HI-poor sequence or in the transition region, as both star formation and supernova feedback are inactive in these galaxies. Moreover, we are largely missing the early-type disk galaxies with small HI disks that are kinematically coupled with the stellar disks (see Section 4.1). We point out that one of the extreme outliers discussed in Section 3.2, NGC 4380 is a highly HI-deficient early-type disk galaxy, which is the only one out of the seven outliers that has no signs of kinematical or morphological abnormalities. These limits on sample completeness will be overcome when we detect and resolve more galaxies with little HI gas content in the upcoming SKA pathfinder surveys.

5 SUMMARY AND CONCLUSIONS

We have learned important new lessons through revisiting the D_{HI}-M_{HI} relation. Firstly, all galaxies are on the D_{HI}-M_{HI} relation regardless of their M_{HI} , M_B , M_{HI}/L_B and D_{HI}/D_{25} . Very importantly, the scatter about the relation is not a function of these properties. This is the first time that we can make such statements thanks to the large and diverse sample compiled here. This result makes the simple D_{HI}-M_{HI} relation provide a strong constraint on galaxy formation models. Perhaps the most important lesson is that there are treasures in the global scaling relations of galaxies which we should not forget to hunt for in this new era of multi-dimensional surveys.

ACKNOWLEDGEMENT

We thank J. Fu, I. Wong, M. Johnson, L. Shao, C. Lagos, B. Catinella for useful discussions. We especially gratefully thank G. Kauffmann for her help in the interpretation of our results. We also thank the anonymous referee for very constructive comments. J.M. van der Hulst acknowledges support from the European Research Council under the European Union's Seventh Framework Programme (FP/2007-2013)/ ERC Grant Agreement nr. 291531.

REFERENCES

- Bahé, Y. M., Crain, R. A., Kauffmann, G., et al. 2016, MNRAS, 456, 1115
- Begum A., Chengalur J. N., Karachentsev I. D., Sharina M. E., Kaisin S. S., 2008, MNRAS, 386, 1667
- Bell E. F., McIntosh D. H., Katz N., Weinberg M. D., 2003, ApJS, 149, 289
- Bigiel F., Leroy A., Walter F., Brinks E., de Blok W. J. G., Madore B., Thornley M. D., 2008, AJ, 136, 2846
- Blitz L., Rosolowsky E., 2006, ApJ, 650, 933
- Braun R., Waltherbos R. A. M., Kennicutt R. C., Jr., Tacconi L. J., 1994, ApJ, 420, 558
- Broeils A. H., Rhee M.-H., 1997, A&A, 324, 877 (B97)
- Brown T., Catinella B., Cortese L., Kilborn V., Haynes M. P., Giovanelli R., 2015, MNRAS, 452, 2479
- Catinella B., et al., 2010, MNRAS, 403, 683
- Chemin L., Carignan C., Foster T., 2009, ApJ, 705, 1395

- Cortese L., et al., 2010, *A&A*, 518, L49
- Chung A., van Gorkom J. H., Kenney J. D. P., Crowl H., Vollmer B., 2009, *AJ*, 138, 1741
- Davé, R., Katz, N., Oppenheimer, B. D., Kollmeier, J. A., & Weinberg, D. H. 2013, *MNRAS*, 434, 2645
- Disney M. J., Romano J. D., Garcia-Appadoo D. A., West A. A., Dalcanton J. J., Cortese L., 2008, *Nature*, 455, 1082
- Donley J. L., Koribalski B. S., Staveley-Smith L., Kraan-Korteweg R. C., Schröder A., Henning P. A., 2006, *MNRAS*, 369, 1741
- Fu J., Kauffmann G., Li C., Guo Q., 2012, *MNRAS*, 424, 2701
- Giovanelli R., et al., 2005, *AJ*, 130, 2598
- Hopkins, P. F., Kereš, D., Murray, N., Quataert, E., & Hernquist, L. 2012, *MNRAS*, 427, 968
- Huang S., Haynes M. P., Giovanelli R., Brinchmann J., 2012, *ApJ*, 756, 113
- Hunter D. A., Wilcots E. M., van Woerden H., Gallagher J. S., Kohle S., 1998, *ApJ*, 495, L47
- Hunter D. A., et al., 2012, *AJ*, 144, 134
- Jaskot A. E., Oey M. S., Salzer J. J., Van Sistine A., Bell E. F., Haynes M. P., 2015, *ApJ*, 808, 66
- Jester S., et al., 2005, *AJ*, 130, 873
- Kalberla P. M. W., Kerp J., 2009, *ARA&A*, 47, 27
- Kauffmann G., Heckman T. M., De Lucia G., Brinchmann J., Charlot S., Tremonti C., White S. D. M., Brinkmann J., 2006, *MNRAS*, 367, 1394
- Kauffmann G., 2014, *MNRAS*, 441, 2717
- Kauffmann G., et al., 2003, *MNRAS*, 341, 54
- Kereš D., Katz N., Fardal M., Davé R., Weinberg D. H., 2009, *MNRAS*, 395, 160
- Kirby, E. N., Cohen, J. G., Guhathakurta, P., et al. 2013, *ApJ*, 779, 102
- Koribalski B. S., 2012, *PASA*, 29, 359
- Koribalski B. S., 2008, *Galaxies in the Local Volume, Astrophysics and Space Science Proceedings*, ISBN 978-1-4020-6932-1. Springer Netherlands, 2008, p. 41
- Kovač K., Oosterloo T. A., van der Hulst J. M., 2009, *MNRAS*, 400, 743 (K09)
- Kreckel K., Platen E., Aragón-Calvo M. A., van Gorkom J. H., van de Weygaert R., van der Hulst J. M., Beygu B., 2012, *AJ*, 144, 16
- Krumholz, M. R., Leroy, A. K., & McKee, C. F. 2011, *ApJ*, 731, 25
- Lagos C. D. P., Baugh C. M., Lacey C. G., Benson A. J., Kim H.-S., Power C., 2011, *MNRAS*, 418, 1649
- Leroy, A. K., Walter, F., Brinks, E., et al. 2008, *AJ*, 136, 2782
- Lelli F., Verheijen M., Fraternali F., 2014, *A&A*, 566, A71
- Lou Y.-Q., Fan Z., 2003, *MNRAS*, 341, 909
- Martinsson T. P. K., Verheijen M. A. W., Bershadsky M. A., Westfall K. B., Andersen D. R., Swaters R. A., 2016, *A&A*, 585, A99
- Matteucci, F., & Chiosi, C. 1983, *A&A*, 123, 121
- Matthews L. D., van Driel W., Monnier-Ragaigne D., 2001, *A&A*, 365, 1
- Meurer G. R., Zheng Z., de Blok W. J. G., 2013, *MNRAS*, 429, 2537
- Mo H. J., Mao S., White S. D. M., 1998, *MNRAS*, 295, 319
- Noordermeer E., van der Hulst J. M., Sancisi R., Swaters R. A., van Albada T. S., 2005, *A&A*, 442, 137
- Ostriker, E. C., McKee, C. F., & Leroy, A. K. 2010, *ApJ*, 721, 975
- Parker E. N., 1969, *SSRv*, 9, 651
- Peng Y.-J., et al., 2010, *ApJ*, 721, 193
- Portas A. M., Brinks E., Filho M. E., Usero A., Dyke E. M., Belles P.-E., 2010, *MNRAS*, 407, 1674
- Roychowdhury S., Huang M.-L., Kauffmann G., Wang J., Chenguang J. N., 2015, *MNRAS*, 449, 3700
- Ryan-Weber E. V., Begum A., Oosterloo T., Pal S., Irwin M. J., Belokurov V., Evans N. W., Zucker D. B., 2008, *MNRAS*, 384, 535
- Ryder S. D., Staveley-Smith L., Malin D., Walsh W., 1995, *AJ*, 109, 1592
- Serra P., et al., 2012, *MNRAS*, 422, 1835
- Serra P., et al., 2014, *MNRAS*, 444, 3388
- Staveley-Smith L., Kim S., Calabretta M. R., Haynes R. F., Kesteven M. J., 2003, *MNRAS*, 339, 87
- Staveley-Smith L., Kim S., Putman M., Stanimirović S., 1998, *RvMA*, 11, 117
- Sternberg, A., Le Petit, F., Roueff, E., & Le Bourlot, J. 2014, *ApJ*, 790, 10
- Swaters R. A., van Albada T. S., van der Hulst J. M., Sancisi R., 2002, *A&A*, 390, 829
- Tremonti, C. A., Heckman, T. M., Kauffmann, G., et al. 2004, *ApJ*, 613, 898
- Verheijen M. A. W., Sancisi R., 2001, *A&A*, 370, 765
- Walter F., Brinks E., de Blok W. J. G., Bigiel F., Kennicutt R. C., Jr., Thornley M. D., Leroy A., 2008, *AJ*, 136, 2563
- Wang J., et al., 2014, *MNRAS*, 441, 2159
- Wang J., et al., 2013, *MNRAS*, 433, 270
- West A. A., Garcia-Appadoo D. A., Dalcanton J. J., Disney M. J., Rockosi C. M., Ivezić Ž., 2009, *AJ*, 138, 796
- Westmeier T., Koribalski B. S., Braun R., 2013, *MNRAS*, 434, 3511
- Westmeier T., Braun R., Koribalski B. S., 2011, *MNRAS*, 410, 2217
- York D. G., et al., 2000, *AJ*, 120, 1579